# Improving sensing properties of entangled carbon nanotube-based gas sensors by atmospheric plasma surface treatment

# Improving sensing properties of entangled carbon nanotube-based gas sensors by atmospheric plasma surface treatment¨

**Neelakandan M. Santhosh[a,b], Aswathy Vasudevan[a,b], Andrea Jurov[a,b], Anja Korent[a,b], Petr Slobodian[c,d], Janez Zavašnik[a], Uroš Cvelbar[a,b,*]**

[a]*Jožef Stefan Institute, Jamova cesta 39, 1000 Ljubljana, Slovenia*

[b]*Jožef Stefan International Postgraduate School, Jamova cesta 39, 1000 Ljubljana, Slovenia*

[c]*Tomas Bata University, University Institute, Centre of Polymer Systems, Tr. T. Bati 5678, 760 01 Zlin, Czech Republic*

[d]*Tomas Bata University, Faculty of Technology, Polymer Centre, T.G.M. 275, 760 01 Zlin, Czech Republic*

[*]*Corresponding author at: Jožef Stefan Institute, Jamova cesta 39, 1000 Ljubljana, Slovenia. E-mail address: uros.cvelbar@ijs.si (U. Cvelbar).*

**ABSTRACT**

Entangled multi-walled carbon nanotubes (MWCNTs) on polyurethane (PUR) after Ar plasma-treatment and He plasma-treatment have been tested as gas sensors for ethanol sensing. It was found that plasma-treated sensors exhibit higher sensitivity compared to the non-treated samples along with different ethanol concentration. Non-treated sensors exhibit similar sensor response with the increase in ethanol concentration, while Ar plasma-treated sensors displays ∼5 times improvement and He plasma-treated sensors show ∼3 times improvement with an increase in ethanol concentration. The sensitivity of the plasma-treated sensors is also stable for following two-weeks after the preparation compared to the non-treated sensor. Entangled nanotube network exhibits a significant shift in the baseline resistance after both plasma-treatments. The response time of the sensor was increased after the plasma-treatment, while the recovery was rather quick. Surface analyses revealed that plasma-treatment did not make any significant morphological changes. Thus, the improvements in stability and sensitivity after plasma-treatment are attributed to the plasma-enhanced surface modification and formation of functional bonds on the surface of nanotubes, which are sensitive to the ethanol vapour.

**Keywords**: Multi-walled carbon nanotubes, plasma-treatment, gas sensor, sensor response, composite

## 1. Introduction

A gas sensor is a device that detects a particular concentration of gases in its environment. Fabrication of gas sensors mainly depends on the application, mostly on the type of gas that should be detected, its concentration and environment. In general, gas sensors should satisfy many requirements such as high stability, selectivity, good responsivity and quick recovery time [**1**]; at the same time the product should be low-cost, made from non-toxic and easy to use materials. Besides this, a sensor that operates at room/low temperatures is in high demand since heating of a sensor is more complex and expensive [**2**]. However, the main challenge for sensors operating at low temperatures remains due to their slow recovery after the sensor response. Along with the requirement for sensors operating at low temperatures, there is a continuous need for high sensitivity, which is dependent on the active surface that the sensing gas can occupy [**1,3-7**]. Recent studies exhibit that improving sensing performance at

low temperatures can be done by using nanostructures [**8-10**], by layering materials [**11-13**] and by modifying surface or inducing hybrid structures [**14-16**]. Unique properties of nanostructures such as gas adsorption capacity due to high surface-to-volume ratio, high structural and thermal stability, high modulation of the electrical charge upon gas exposure, and the possibility of changing the electrical properties by surface modifications can be used for improving the stability and sensitivity of the sensors [**17**]. Mostly, nanomaterial-based gas sensors are made of metal oxides, carbon nanotubes and graphene. Among them, CNTs possess quick response time, high sensitivity, good reversibility and stability [**18**].

CNTs are composed of graphene layers rolled into cylindrical geometry, which is classified as single-walled carbon nanotubes (SWCNT) composed of a single layer of graphene and multi-walled carbon nanotubes (MWCNT) composed of multiple layers of graphene with the same central axis [**1**]. Depending on the tube diameter and chirality, SWCNT can either be metallic or semiconducting in which case they are p-type semiconductors [**17**]. However, pure crystalline SWCNTs are inert to some volatile organic gases. In the case of MWCNT gas adsorption happens on the outer surface where a molecule connects with the sensor with Van der Waals forces. The molecule changes the electrical charge flow in the sensor, which can be measured as the change in the sensor resistivity [**19**]. In the case of adsorption of oxidising gas molecules on sensors surface, the electric resistance of CNT decreases with the number of adsorbed gas molecules, due to the creation of additional positive holes as an electric current carrier and vice versa [**20**]. Moreover, sensor response or other sensor properties can be improved by modifying the structure and morphology of the CNTs by combining with different nanostructures [**17,21-23**], by adding a transition metal [22], by plasma-treatment [**19,24-27**], etc. Compared to other surface modification techniques, plasma-treatment gives the possibility of defect generation and surface functionalisation of CNTs simultaneously, which can be controlled by plasma and treatment conditions. Research done with the plasma-enhanced surface modification of CNTs suggests that both, low and atmospheric pressure plasma can be used for the surface treatment to improve the stability and sensitivity. Depending on the sensor material, one can choose proper plasma type and plasma parameters for the surface modification. These treatment techniques allow changing the chemical composition of the CNT surface without destructing the morphology. Besides the functionalising gases, plasma generated by inert gases such as helium and argon provides higher ion bombardment and creates defects on the CNT surface due to the plasma-assisted etching. Furthermore, plasma-treatment can introduce free electrons to the sensor structure or creating free bonds inside the material, thus making them more sensitive when exposed to analyte vapours.

A variety of CNT based gas sensors are already reported to detect alcohols, where the sensing properties are improved by depositing metal oxides, metals and organic molecules. Among all the alcohol-based sensors, ethanol gas sensors are of considerable interest. Ethanol ($C_2H_5OH$) is a volatile, flammable, colourless organic compound (VOC) detrimental to the environment, plants, organisms and people [**18,23**]. Additionally, detection of ethanol fumes is essential in industries, alcohol storage facilities, fruit transportation, and many more. Ethanol is reductive, and when adsorbed on CNT surface, its electrons occupy positively charged holes and consequently increase the resistivity of the material [**23,28-31**], which results in the p-type sensor response.

In this work, we have designed a simple sensing device using entangled COOH-functionalised MWCNTs for the detection of ethanol at room temperature. Additionally, the effect of atmospheric pressure plasma-treatment on the CNTs using inert gases for improving the sensing properties were investigated. Also, we presented a systematic study on the changes in response and recovery time of the sensors by the effect of plasma-assisted surface modification. The gas sensors were prepared by simple vacuum filtration of MWCNTs on polyurethane (PUR) membrane to form entangled MWCNT

sensor, and then they were treated with Ar or He plasma generated at atmospheric pressure. Changes in sensitivity of all sensors were measured by two-point electrical measurements while using ethanol vapours as the target gas. Stability of all prepared sensors was investigated by repeating all the measurements after two weeks. Structural and morphological analysis were obtained by Raman spectroscopy and scanning electron microscopy (SEM) analysis. Changes in the functional entities of the sensors were investigated using Fourier Transform Infrared (FTIR) spectroscopy. Finally, all the results were considered to explain the effect of inert gas plasma-treatment at atmospheric conditions on the sensing properties of entangled MWCNTs.

## 2. Experimental methods

### *2.1. Gas sensor preparation*

Preparation of bucky paper (BP) was done by a vacuum filtration technique and reported elsewhere [**32**]. A surfactant solution of pH $\approx$ 10 was prepared with 46.2 g sodium dodecyl sulphate (Sigma-Aldrich), and 0.14 M water solution of pentanol (Alfa Aesar) in 300 ml deionised water. Separately, 0.8 g of 8% COOH-functionalised MWCNT (Sigma-Aldrich, average diameter x length is 9.5 nm x 1.5 $\mu$m) was weighed out and mixed with 250 ml deionised water. The above-prepared surfactant solution and MWCNT-water suspensions were mixed and sonicated for 1 h at room temperature to ensure the fine dispersion of MWCNTs. The suspension was vacuum filtrated through a PUR membrane (GSM 3 g/m$^2$, Pardam Nanotechnology, Czech Republic) to achieve a flat homogeneous sheet of entangled carbon nanotubes with a thickness of 0.03 ± 0.02 mm, also called the BP (Fig.S1 (a)). To remove the impurities, BP was washed several times with ethanol and distilled water. Prepared BP was left to dry overnight at room temperature. Finally cuts 1.5 x 1.5 cm from prepared BP to fabricate the gas sensors.

### *2.2. Plasma-treatment*

Since the PUR membrane is a temperature-sensitive material, low-temperature atmospheric pressure plasma jet (APPJ) was used for the surface treatment to improve the sensitivity. APPJ system consisted of a single copper electrode without grounding and was powered by a kHz high-voltage signal source. This system allows smooth operation and produces low-temperature plasma, which is suitable for the temperature-sensitive sensors. Inert gases such as argon and helium were used to generate plasma. Compared to mono-functional specific grafting using specific gases like $NH_3$, $O_2$ or $N_2$; atmospheric pressure plasma-treatment using inert gases allows the possibility of surface functionalisation by the functional groups present in the atmosphere [**33,34**]. Surface treatment was carried out with a gas flow rate of 100 sccm for a fixed time of 3 min. The distance between the sensor and the exit of the APPJ's orifice was fixed at 2.5 cm, meaning that the sensors were treated in the after-glow region of the plasma. Plasma dissipated over the surface, and uniform treatment is assumed.

### *2.3. Electrical and gas sensing characterisation*

I-V characteristics of the sensors were measured by an easy two-point method. We forced a voltage (0-10 V) and measured the current. The gas sensor properties were determined by measuring the change in resistance of sensor during the sensing experiment by a two-point method using a Keithley 2460-high current source meter at a constant input current of 10 mA. Ethanol (ACS reagent for analysis) was used as the sensing gas for investigating the effect of plasma surface treatment on the

gas sensor sensitivity. 5 ml volume of ethanol was measured and transferred to a conical flask of 250 ml capacity, and the rest of the flask was filled with ambient air. The sensor was placed to the saturated vapour above the ethanol liquid during the sensing cycle (gas in phase) and placed to an identical conical flask of 250 ml filled with air during the recovery process (gas off phase). The gas in and gas off during the sensing measurements were assigned with an interval of 180 s. The measurements were performed at different temperatures, starting from the room temperature (20 ± 2 °C), then at 35, 50 and 65 °C. The sensor response was calculated using the following equation:

$$\text{Sensor Response} = \frac{R_g - R_a}{R_a} \quad (1)$$

where $R_g$ is the resistance of a sensor after inserting ethanol and $R_a$ is the resistance of the sensor in air. The concentration $C_{et}$ of ethanol, inside the sensing chamber was controlled by heating the ethanol volume to different temperatures. Since the sensing chamber is filled with a mixture of gases (air and ethanol vapour), Dalton's law was used for the estimation of volume-based concentration of ethanol as per the following equation:

$$p_{et} = p_{tot}\, c_{et} \quad (2)$$

where $p_{et}$ is the vapour pressure of ethanol, $p_{tot}$ is atmospheric pressure (101,325 kPa) and $c_{et}$ is the volume-based concentration of ethanol. Calculation of ethanol vapour pressure is well researched, and the values for specific temperatures can be obtained from many databases. In this study, we have used the vapour pressure described in Dortmund Data Bank (**http://www.ddbst.com/en/EED/PCP/VAP_C11.php**) for the calculation of ethanol concentration. The volume-based concentration of ethanol is estimated as 5.71% at 20 °C, 13,58% at 35 °C, 29,1% at 50 °C, and 57,68% at 65 °C. The concentration is increased by approximately 50% from room temperature to the highest temperature, which opens up an opportunity to explore the influence of ethanol concentration on the sensing measurements. Schematic diagram of the experimental setup was shown in **Fig. S1**(b). The stability of the prepared sensors was investigated by conducting all the measurements after two weeks.

*2.4. Characterisation techniques*

Surface morphology of the gas sensors was characterised by SEM analysis (JSM-7600F and JSM-5800, Jeol Inc.), operating at an acceleration voltage 10 kV. Chemical and phase composition of the samples were analysed by transmission electron microscope (TEM, JEM-2010F, Jeol Inc.) operating at 200 kV. The micrographs were recorded by a slow-scan CCD camera (Orius SC1000, Gatan). Raman spectra of the sensors were recorded using NTEGRA confocal Raman spectrometer at an excitation wavelength of 633 nm with an incident power ~ 3 mW and objective of 20x at a spot size of 10 $\mu$m. The spectrum was recorded at three different spots of each sensor to eliminate the variations and investigated the structural changes after the plasma-treatment. FTIR spectrum was recorded to analyse the changes in the functional entities of the sensors before and after plasma-treatment using Spectrum GX FTIR spectrometer by Perkin Elmer that was equipped with a photoacoustic detector with 64 scan runs average at 8 $cm^{-1}$. All the analysis was done right after the sensor preparation and repeated two weeks later to monitor the ageing effect.

## 3. Results and discussion

### *3.1. Resistance measurements*

The resistance of the as-prepared sensor was measured as (1041 ± 5) Ω. However, the resistance of the sensor is decreased to (702 ± 7) Ω after He plasma-treatment and to (553 ± 10) Ω after Ar plasma-treatment. In addition to the decrease in the resistance, the stability of the resistance after the plasma-treatment should also be noted. **Fig. 1** (a) exhibits the steadiness of the resistance of both the non-treated and plasma-treated sensors at the room temperature (20 ± 2 °C). The significant change in the resistance might be due to the surface modification either by plasma-enhanced etching or by the functionalisation of CNT surface. Typical current-voltage (I-V) characteristics of the non-treated and plasma-treated sensors at room temperature are presented in **Fig. 1** (b). The linear I-V relationship confirms the ohmic nature of the sensors.

The repeatability of the sensing cycle of the sensors was checked at different concentration of ethanol by heating at different temperatures as 20 °C, 35 °C, 50 °C and 65 °C, and the stability of the sensor was investigated by repeating all the measurements after two weeks. The sensor response measurements are presented in **Fig. 2**, which suggests that the plasma-treated sensors acquired more stable sensor response than the non-treated sensor. The non-treated sensor possesses an unstable response at room temperature, which slightly turns into a stable response with an increase in temperature. Nevertheless, the change in the sensor response with temperature is not significant. In the case of both plasma-treated sensors, the sensor response became stable and increased with the temperature. He plasma-treated sensors possess similar sensor response at low-temperature, which increases with the temperature and attained ∼3 times improvement at 65 °C. Whereas Ar plasma-treated sensors exhibit a substantial improvement of sensor response (∼5 times) even at low-temperature and increase with the temperature. A higher concentration of analyte after heating makes the sensor more stable during the sensing cycle. However, the stability studies after two weeks indicated that the maximum response of all the sensors were decreased, especially for non-treated and He plasma-treated sensors.

Average of maximum sensor response was calculated to understand more about the response and repeatability of the sensors changing with temperature. This response is presented in **Fig. 3**, where the average response of the sensors at different concentration of ethanol (at each temperature calculated using Eq. (**2**)) at as-prepared and two weeks later conditions. At higher concentrations of ethanol (increase with the elevation of temperature), plasma-treated sensors show better response than the non-treated sensor. Among all the tested sensors, the non-treated sensor exhibits a constant sensor response for all concentrations. For He plasma-treated samples, the response was almost similar to the non-treated sensor but slightly improved with higher concentrations. The highest sensor response was shown by Ar plasma-treated sensor, which could be attributed to the greater extent of surface modifications done by the Ar plasma. However, the stability studies on the average response after two weeks suggest that the maximum sensor response of all the sensors become lower than the as-prepared conditions. In the case of non-treated and He plasma-treated sensors, the sensor response was negligible after two weeks, even when the ethanol concentrations increased. On the other hand, Ar plasma-treated samples disclosed a stable response after two weeks and the sensor response increases with increasing the ethanol concentration.

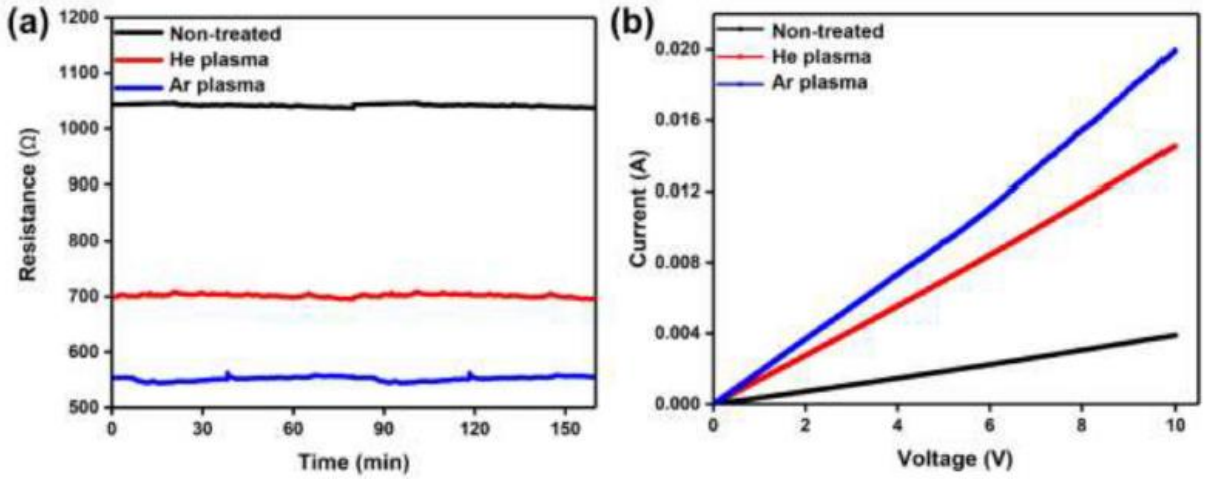


**Fig. 1**. (a) The stability of the resistance of the prepared sensors at room temperature, (b) I-V characteristics of the non-treated and plasma-treated sensors.

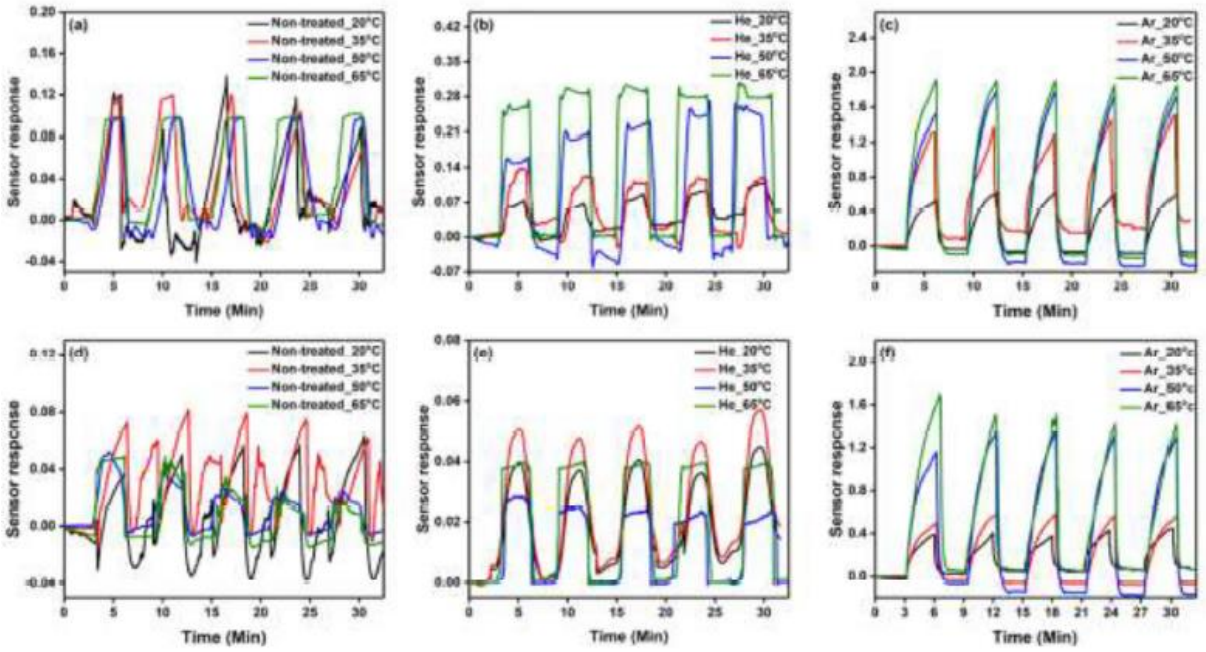


**Fig. 2**. The repeatability of vapour detection on (a) non-treated and (b) He plasma-treated and (c) Ar plasma-treated sensors; and corresponding measurements of stability in performance after two weeks for (d) non-treated, (e) He plasma-treated and (f) Ar plasma-treated sensors.

The response and recovery curve of the sensors are presented in Fig. 4. The gas in and gas off during the sensor measurements are assigned with an interval of 180 s. The results show that the Ar plasma-treated sensors have higher sensor response, and the recovery to the initial resistance is quicker for the non-treated and He plasma-treated sensors. These results indicate that Ar plasma-treatment has made significant changes in the properties of sensor. Moreover, Ar plasma-treated sensors appear to be the most stable in both response and recovery even after two weeks. On the contrary, the non-treated sensor displays a behaviour where the response drops instantaneously to the value below the initial resistance and then recovers to the original value after the gas off. The response and recovery appear to be better after two weeks, which could be explained by the surface interaction with the surroundings. However, He plasma-treated sensors have much longer recovery time than the response

time. Since the change in sensor response is minimal, it implies that the capability of the sensor to adsorb ethanol vapour is comparatively low even after the plasma-treatment. During the recovery, the resistance falls below the original value and then recovered to the initial value similar to non-treated sensor. However, the response curves after two weeks displays similar behaviour as the initial response.

A comparison between the response and recovery times of all the sensors at the room temperature is given in **Fig. 5**. The response time $T_{res}$, of the sensors, was defined as the time taken to achieve 90% of the maximum change in resistance. In contrast, recovery time $T_{rec}$ was calculated as the time taken to recover to 90% of the initial resistance from the maximum resistance change occured during the sensing cycle. A schematic explanation for the calculation of $T_{res}$ and $T_{rec}$ from our results is shown in Fig. S2. It was observed that the as-prepared He plasma-treated sensor had the fastest response time of 114 s, whereas the highest response time of 152 s was observed for Ar plasma-treated sensor.

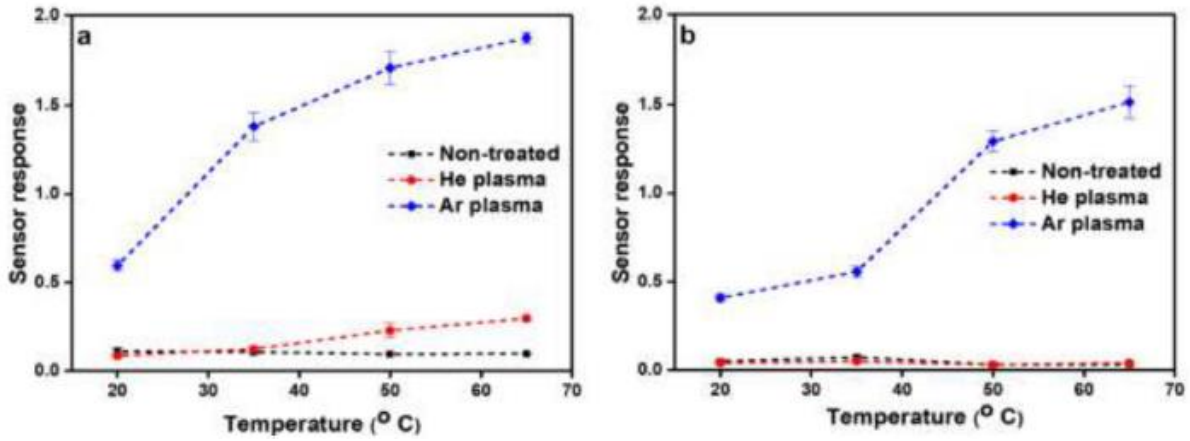


**Fig. 3**. The average sensor response compared to the concentration of ethanol for all the sensors (a) as-prepared and (b) two weeks later.

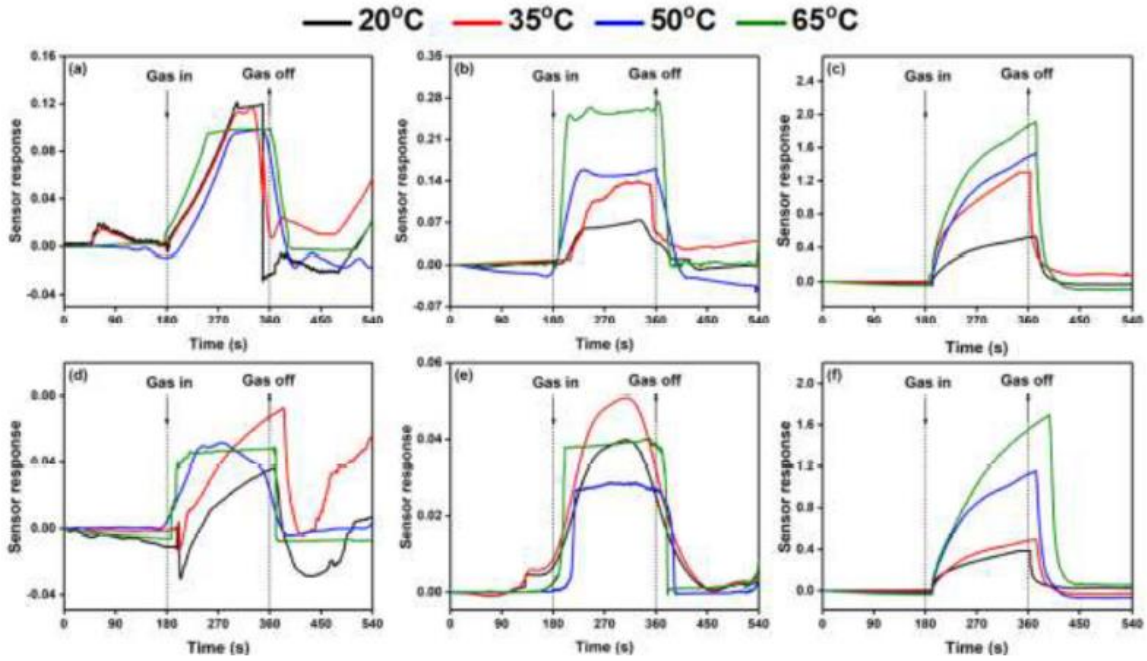


**Fig. 4**. The response curve for the first sensing cycle of the sensors at different temperatures: (a) non-treated, (b) He plasma-treated and (c) Ar plasma-treated; two weeks later: (d) non-treated, (e) He plasma-treated and (f) Ar plasma-treated sensors.

On the other hand, in the case of recovery, Ar plasma-treated sensor had the fastest recovery time of 40 s, where the non-treated sensor was displayed the slowest recovery time of 152 s. After two weeks, the non-treated sensors took the longest time to respond as well as to recover (156 s and 142 s respectively). He plasma-treated sensor had the fastest response of 88 s and Ar plasma-treated sensor demonstrates the fastest recovery time of 79 s. These results are indicating that the different plasma-treatments using inert gases are causing different effects on the surface of sensors, which allows tuning the gas sensing properties.

Since both the electrical resistance and sensing properties of the sensors change with plasma-treatment, which also varies after two weeks of repeated measurements, sensors required a detailed investigation of the structural and morphological changes. Thus, the surface of sensors was analysed with different characterisation techniques to get a better insight into the effect of plasma surface treatment.

### *3.2. Morphology analysis*

To analyse surface modifications of all non-treated and plasma-treated samples, SEM was used, and the results are presented in **Fig. 6**. Nanotubes did not seem to be affected by plasma, and no visual damages were observed on the entangled structure (Fig. S3 and S4), which means that the surface of sensors is the same before and after the plasma-treatment.

Detailed TEM and HR-TEM analysis were done to get an insight into the changes that occurred on the surface of BPs after plasma-treatment (**Fig. 7** (a-c)).

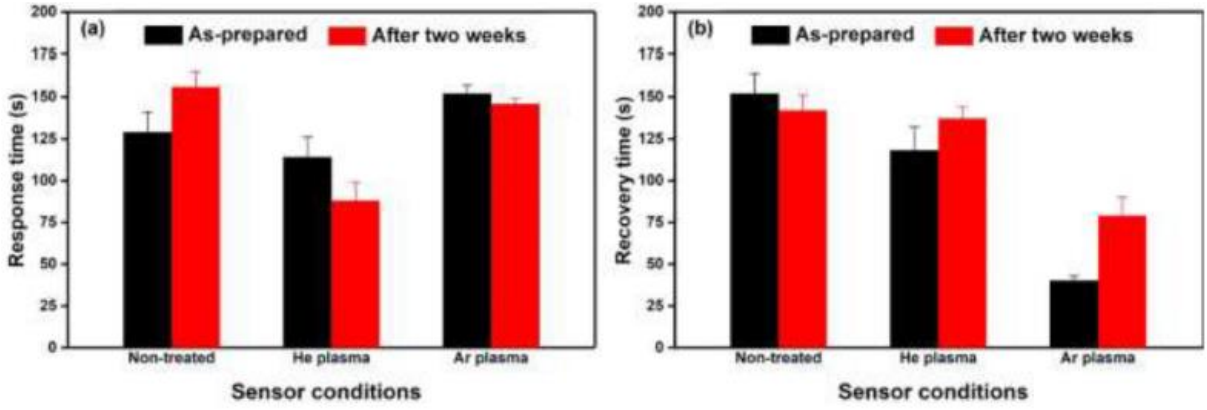


**Fig. 5**. Comparison of sensor (a) response time and (b) recovery time of non-treated, He plasma-treated and Ar plasma-treated sensors at the room temperature.

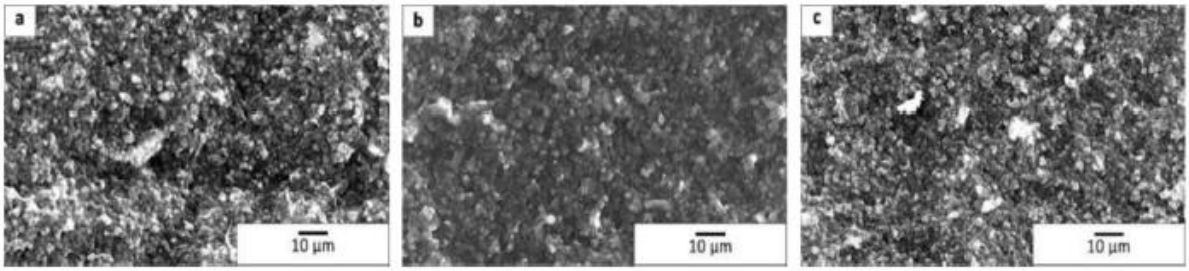


**Fig. 6**. Characteristic SEM micrographs of (a) non-treated, (b) He and (c) Ar plasma-treated sensor surface.

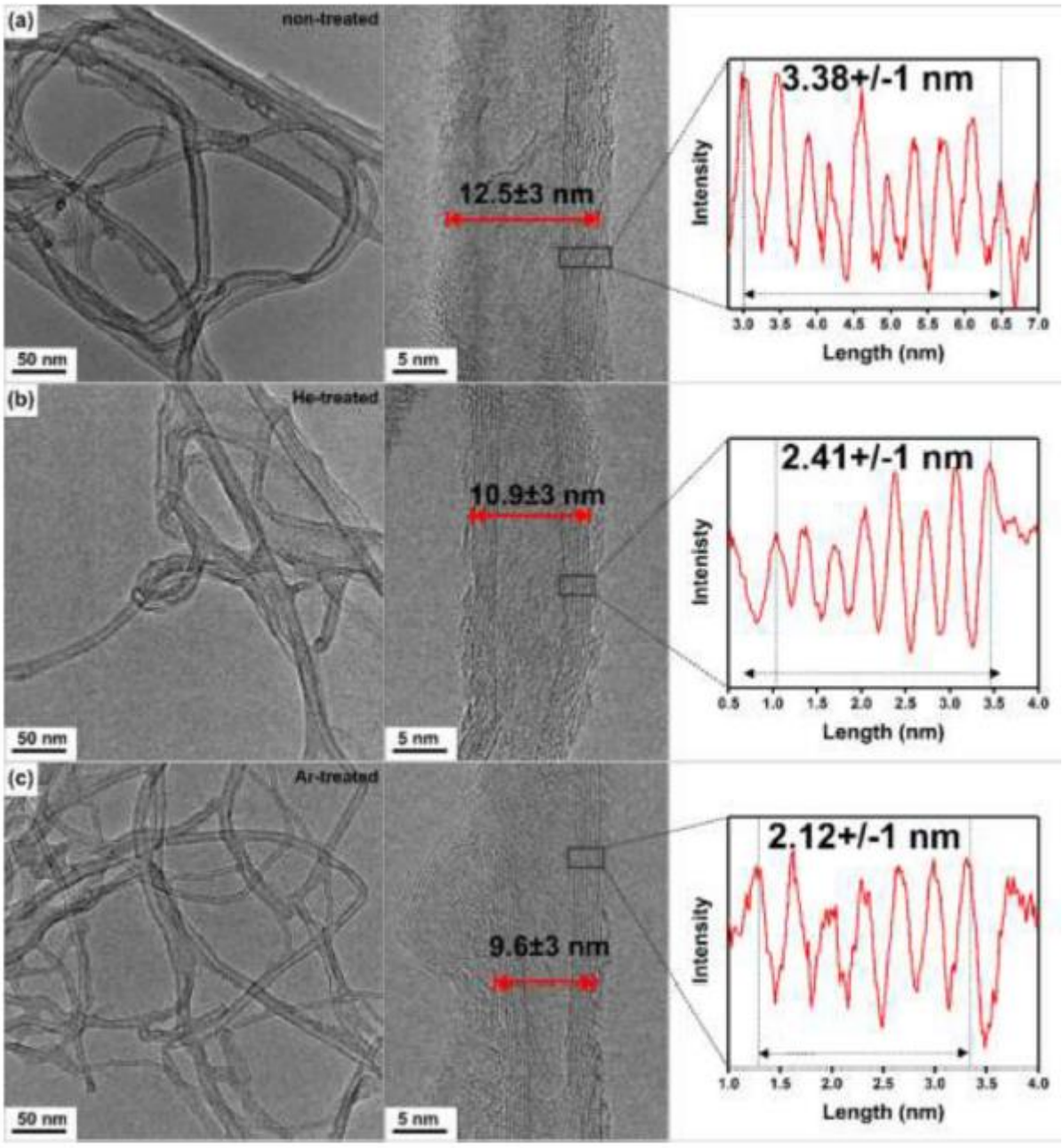


**Fig. 7**. Overview and high-resolution TEM micrographs of carbon nanostructures and intensity profile from the marked area of the (a) non-treated, (b) He-treated and (c) Ar treated sensor.

The individual nanotubes are multi-walled with an average diameter of 10-15 nm. The surface of the nanotubes is covered with a wrinkled amorphous layer of carbon. The diameter of the nanotubes in the non-treated sensor was 12.57 ± 3 nm, and it was reduced to 10.9 ± 3 nm after He plasma-treatment and 9.6 ± 3 nm after Ar plasma-treatment. This slight reduction in the diameter can be ascribed to the plasma-enhanced etching effect, which also affects the thickness of the carbon layers. The intensity profile obtained from the carbon layers (**Fig. 7** (a-c)) is indicating that the layer thickness is also slightly decreasing with plasma-treatment, which can be due to the removal of the top layer. Additionally, the continuous amorphous wrinkled layer visible on the non-treated sensor is completely removed after He plasma-treatment and partially removed after the Ar plasma-treatment. These effects can improve

the conductivity of the BPs after the plasma-treatment and enhance the interaction of the carbon layer with ethanol vapour during the sensor cycle, which in turn improve the response of the sensor.

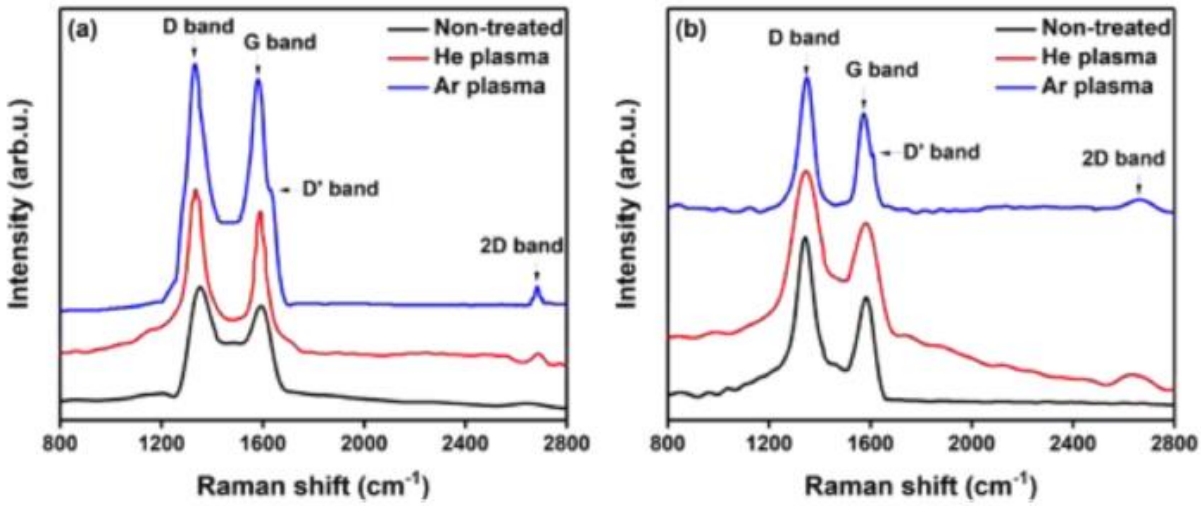


**Fig. 8**. Raman spectra of the non-treated, He and Ar plasma-treated sensors (a) as-prepared and (b) two weeks later.

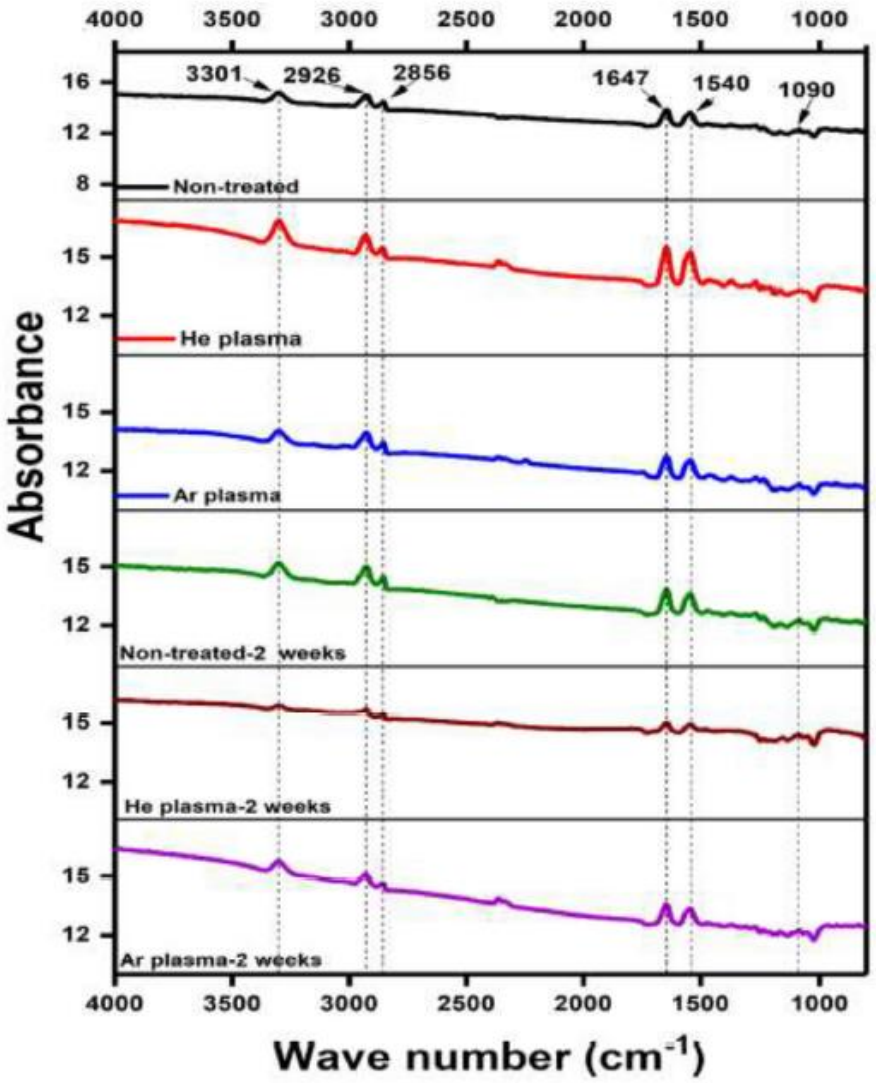


**Fig. 9**. FTIR spectra of the non-treated, He plasma-treated and Ar plasma-treated sensors

*3.3. Raman spectroscopy*

Raman spectroscopy was used for the qualitative characterisation of structural defects in CNTs, by comparing the ratio between the intensities of the defect and graphitic bands. The results of this analysis are presented in **Fig. 8**. The Raman spectra of the non-treated sensor display two well-distinguished peaks approximately at 1343 $cm^{-1}$ and 1587 $cm^{-1}$, D and G peak, respectively, which are the typical characteristics of graphitic carbon. The D peak is induced by the disorder or defect due to the distortion of graphite lattice [**35-37**] and the G peak forms due to the crystallite graphite [**38**]. There was no 2D band (around 2675 $cm^{-1}$) observed in the Raman spectrum of the non-treated sensor, which is the second-order two-phonon process in a graphitic $sp^2$ material and indicates that the disordered graphene layers were overlapped with plenty of oxygenated functional groups. Lack of this peak indicates that the non-treated sensors possess more amorphous behaviour than the treated ones. The Raman characteristics of sensors were changed both with He and Ar plasma-treatments. The D peak is shifted to 1338 $cm^{-1}$ and 1336 $cm^{-1}$ after He and Ar plasma-treatment, respectively, which could be due to the formation of reactive edges on CNTs caused by plasma etching [**39**]. The evolution of a 2D band that was observed after He and Ar plasma-treatment around 2678 $cm^{-1}$ and 2673 $cm^{-1}$ indicates that the plasma-treatment causes the removal of amorphous carbon from the surface and progression of more graphitic behaviour. There was an additional shoulder peak observed along with the G peak at 1618 $cm^{-1}$ after the Ar plasma-treatment, which is known as D' peak, a disorder peak frequently seen in microcrystalline graphite usually produced from the thin edges of graphitic layers.

Comparison of the $I_D/I_G$ ratio of different sensors exhibits the change in structural quality. The $I_D/I_G$ ratio for the as-prepared sensor was 1.1, which slightly decreases to 1.09 after He plasma-treatment and further decreases to 1.03 after Ar plasma-treatment. These results imply that the defect density of CNTs decreases with the plasma-treatment by the etching of disordered carbon atoms. There is no significant change observed in the Raman spectrum after two weeks, which means there is no substantial change in the structure of the sensors. Considering the changes observed in the TEM micrographs and Raman characteristics of the sensors, the improvement in sensor properties can be explained as the improvement in graphitic behaviour of sensors after the plasma-treatment.

*3.4. Fourier-transform infrared spectroscopy*

FTIR analysis was carried out to understand the effect of plasma-treatment on the functional entities (**Fig. 9**). All the spectra exhibit similar characteristic behaviour with akin vibrations of functional entities. The distinct peak around 3301 $cm^{-1}$ refers to the O—H stretching of the hydroxyl group, that may arise from the oscillation of the carboxyl group. The peaks at 2926 $cm^{-1}$ and 2856 $cm^{-1}$ can be associated with the symmetric and asymmetric stretching of C—H group. The peak observed at 1647 $cm^{-1}$ can be due to the stretching of the carbon nanotube backbone [**40**]. The peak signal formed at 1540 $cm^{-1}$ was due to the stretching of C=C group in the CNTs [**41**]. A weak peak observed at 1090 $cm^{-1}$ could be assigned to O—H bending deformation mode of the carboxyl groups [**42**]. The peak intensities of functional groups increased after the plasma-treatment, which indicates the increased surface functionalisation. Additionally, a peak at 2360 $cm^{-1}$ was observed after the plasma-treatment, which corresponds to the stretching of carbon dioxide. A small peak at 2245 $cm^{-1}$ appeared only in the Ar plasma-treated sensor and is attributed to the stretching of nitrile or alkynes groups. Also, the change of different weak peaks is observed in the range of 1500-1100 $cm^{-1}$ for plasma-treated sensors that could arise because of the bending of alkane and aldehyde groups attached to the CNT network. However, the intensity of all the peaks from the He plasma-treated sensor decreased after two weeks, which shows that the stability of the sensor changed with time. Whereas, the intensity of the Ar

plasma-treated sensor did not change significantly, which implies its better stability. Since all the sensors show almost similar infrared spectrum, the difference observed in the sensor response after plasma-treatment is mostly associated with the vibrations of either improved graphitic behaviour or O-terminated and H-terminated functional groups, which can enhance the sensitivity of the prepared sensors.

**4. Mechanism of ethanol sensing and the influence of plasma-treatment**

The non-treated sensor shows a poor and irregular sensor response that improved and stabilised after the plasma-treatment, which may be due to the interaction of plasma-activated species with the surface of carbon nanotubes. Atmospheric pressure plasma surface treatment causes the removal of amorphous carbon, the formation of H/O-ter-minated groups and dangling bonds, all of which are improving the absorption of ethanol molecules to the surface of the sensor. No significant morphological changes observed from SEM images confirm the capability of plasma-treatment for improving the performance without any structural damage. Detailed analysis by TEM is suggesting that the plasma-treatment leads to the removal of amorphous wrinkled structures from the nanotube surface, which eventually improves the crystalline behaviour of the carbon nanostructures. Raman and FTIR spectra analysis are also confirming that the plasma-treatment mainly improves the graphitic behaviour of the CNTs rather than causing significant chemical modification. Improvement in the graphitic characteristics can be attributed to the plasma-enhanced etching by creating vacancies with the removal of amorphous carbon, which finally improves p-type conductivity of the sensor. Moreover, removal of the amorphous structures from the outer layer of the individual nanotube surface can enhance the adsorption of ethanol to the carbon nanotube and they donate electrons to the conduction state, which increases resistance. The removal of the amorphous structure is more prominent after Ar plasma-treated sensors, in which higher ethanol vapours were adsorbed to the nanotubes and shows higher response compared to other sensors. The other possible reason for the increase of resistance is the change of contact resistance between individual nanotubes and increases the macroscopic resistance of the sensor. The sensor performance after Ar and He plasma-treatment is vividly different and indicating that plasma surface modification using various inert gases at atmospheric conditions is also considerably different. Considering Ar and He as inert gases, the surface functionalisation is only carried out by the excitation of functional groups present in the atmospheric conditions. There is no considerable change in FTIR spectra, suggesting that state of functionalisation after the plasma-treatment is similar before and after plasma-treatment. Thus, the significant factor that influences the surface modification is the bombardment of plasma species on the CNT surface, which affect the electrical conductivity of the sensors. Compared to helium, argon is much heavier and carries more reactive species to the surface of the sensor and creates severe surface modifications by plasma-enhanced etching which results in the formation of more conductive channels. Also, the stability measurements of the sensors show that the changes made by Ar plasma-treatment are persistent even after two weeks but not in the case of He plasma-treatment. Based on the analysis of the experimental data, we can conclude that plasma-treatment makes the sensors more sensitive to the environment. Moreover, the stability of the sensors after plasma-treatment can be recognised as the formation of stable defect channels facilitating the ethanol vapours to access all parts of the sensor. In plasma-treated samples, the dangling bonds, which are formed by the plasma-treatment, might be responsible for the enhanced sensing properties.

## 5. Conclusion

It was found that the sensitivity to ethanol vapours of the entangled COOH-functionalised MWCNTs networks was improved by the atmospheric pressure plasma-treatment using inert gases. The resistance of the sensors was decreased after the plasma-treatment. All the sensors were able to detect the ethanol vapour, whereas the non-treated sensor exhibits an inferior sensing ability. Sensor response and stability of the He plasma-treated samples were improved by 3 times, and that of Ar plasma-treated samples were improved by 5 times with an increase in ethanol concentration. Evaluation of response time and recovery time shows that the time of response increased after the plasma-treatment due to the higher sensor response while the time of recovery was fast. Surface morphology analysis confirms that the plasma-treatment did not destroy the tubular structure of CNTs. Raman spectra and TEM analysis confirm the improvement of graphitic behaviour after the plasma-treatment. Infrared spectrum suggests similar bond vibrations for all the sensors, but the presence of additional peaks after plasma-treated sensors indicates the improved functional entities in the CNT network. It is evident that the plasma-treatment improves the graphitic nature of nanotubes, the formation of defects, and the presence of functional groups of the sensors, which is enhancing the sensing properties. Exploring the selectivity of the prepared sensor towards different gases needs to be investigated for the future applications of the entangled carbon nanotube-based sensors.

## References


[1] J.T.W. Yeow, Y. Wang, A review of carbon nanotubes-based gas sensors, J. Sensors. (2009), https://doi.org/10.1155/2009/493904.

[2] W. Yu, Y. Sun, T. Zhang, K. Zhang, S. Wang, X. Chen, N. Dai, CuO/WO3 hybrid nanocubes for high-responsivity and fast-recovery H2S sensors operated at low temperature, Part. Part. Syst. Charact. 33 (2016) 15-20, https://doi.org/10.1002/ ppsc.201500178.

[3] B.S. Dakshayini, K.R. Reddy, A. Mishra, N.P. Shetti, S.J. Malode, S. Basu, S. Naveen, A.V. Raghu, Role of conducting polymer and metal oxide-based hybrids for applications in ampereometric sensors and biosensors, Microchem. J. (2019), https:// doi.org/10.1016/j.microc.2019.02.061.

[4] N.P. Shetti, S.J. Malode, D. Ilager, K. Raghava Reddy, S.S. Shukla, T.M. Aminabhavi, A novel electrochemical sensor for detection of molinate using ZnO nanoparticles loaded carbon electrode, Electroanalysis (2019), https://doi. org/10.1002/elan.201800775.

[5] N.P. Shetti, S.D. Bukkitgar, K.R. Reddy, C.V. Reddy, T.M. Aminabhavi, Nanostructured titanium oxide hybrids-based electrochemical biosensors for healthcare applications, Colloids Surf. B: Biointerfaces (2019), https://doi.org/10. 1016/j.colsurfb.2019.03.013.

[6] P. Slobodian, U. Cvelbar, P. Riha, R. Olejnik, J. Matyas, G. Filipič, H. Watanabe, S. Tajima, H. Kondo, M. Sekine, M. Hori, High sensitivity of a carbon nanowall-based sensor for detection of organic vapours, RSC Adv. (2015), https://doi.org/10. 1039/c5ra12000d.

[7] G. Filipič, J. Gruenwald, Temperature influence on the diethylamine sensing abilities of CuO nanoparticles deposited by atmospheric pressure plasma, J. Technol. Sp. Plasmas. (2020), https://doi.org/10.31281/jtsp.v1i1.10.

[8] H.G. Moon, Y.S. Shim, D.H. Kim, H.Y. Jeong, M. Jeong, J.Y. Jung, S.M. Han, J.K. Kim, J.S. Kim, H.H. Park, J.H. Lee, H.L. Tuller, S.J. Yoon, H.W. Jang, Selfactivated ultrahigh chemosensitivity of

oxide thin film nanostructures for transparent sensors, Sci. Rep. (2012), https://doi.org/10.1038/srep00588.

[9] X. Pan, X. Zhao, J. Chen, A. Bermak, Z. Fan, A fast-response/recovery ZnO hierarchical nanostructure based gas sensor with ultra-high room-temperature output response, Sensors Actuators B Chem. 206 (2015) 764-771, https://doi.org/10. 1016/j.snb.2014.08.089.

[10] D. Zhang, Z. Liu, C. Li, T. Tang, X. Liu, S. Han, B. Lei, C. Zhou, Detection of NO2 down to ppb levels using individual and multiple In2O3 nanowire devices, Nano Lett. (2004), https://doi.org/10.1021/nl0489283.

[11] Y. Zhou, G. Xie, T. Xie, H. Yuan, H. Tai, Y. Jiang, Z. Chen, A sensitive film structure improvement of reduced graphene oxide based resistive gas sensors, Appl. Phys. Lett. (2014), https://doi.org/10.1063Z1.4890843.

[12] F. Niefind, W. Bensch, M. Deng, L. Kienle, J. Cruz-Reyes, J.M. Del Valle Granados, Co-promoted MoS2 for hydrodesulfurization: new preparation method of MoS2 at room temperature and observation of massive differences of the selectivity depending on the activation atmosphere, Appl. Catal. A Gen. (2015), https://doi.org/ 10.1016/j.apcata.2015.03.003.

[13] J.D. Fowler, M.J. Allen, V.C. Tung, Y. Yang, R.B. Kaner, B.H. Weiller, Practical chemical sensors from chemically derived graphene, ACS Nano (2009), https://doi. org/10.1021/nn800593m.

[14] M. Zhao, J.X. Huang, C.W. Ong, Room-temperature resistive H 2 sensing response of Pd/WO 3 nanocluster-based highly porous film, Nanotechnology. 23 (2012) 315503, https://doi.org/10.1088/0957-4484/23/31/315503.

[15] H.T. Wang, B.S. Kang, F. Ren, L.C. Tien, P.W. Sadik, D.P. Norton, S.J. Pearton, J. Lin, Hydrogen-selective sensing at room temperature with ZnO nanorods, Appl. Phys. Lett. (2005), https://doi.org/10.1063/1.1949707.

[16] Z.S. Hosseini, A. Mortezaali, A. Iraji Zad, S. Fardindoost, Sensitive and selective room temperature H2S gas sensor based on Au sensitized vertical ZnO nanorods with flower-like structures, J. Alloys Compd. (2015), https://doi.org/10.1016/]'. jallcom.2014.12.163.

[17] T. Zhang, S. Mubeen, N.V. Myung, M.A. Deshusses, Recent progress in carbon nanotube-based gas sensors, Nanotechnology. (2008), https://doi.org/10.1088/0957-4484/19/33/332001.

[18] K. Xu, C. Fu, Z. Gao, F. Wei, Y. Ying, C. Xu, G. Fu, Nanomaterial-based gas sensors: a review, Instrum. Sci. Technol. (2018), https://doi.org/10.1080/10739149.2017. 1340896.

[19] A. Zandi, A. Gilani, H. Ghafoori fard, J. Koohsorkhi, An optimized resistive CNT-based gas sensor with a novel configuration by top electrical contact, Diam. Relat. Mater. (2019), https://doi.org/10.1016/j.diamond.2019.01.020.

[20] H. Elhaes, A. Fakhry, M. Ibrahim, Carbon nano materials as gas sensors, Mater. Today Proc, 2016, https://doi.org/10.1016/j.matpr.2016.04.166.

[21] D.R. Kauffman, A. Star, Carbon nanotube gas and vapor sensors, Angew. Chem. Int. Ed. (2008), https://doi.org/10.1002/anie.200704488.

[22] S. Brahim, S. Colbern, R. Gump, A. Moser, L. Grigorian, Carbon nanotube-based ethanol sensors, Nanotechnology 20 (2009), https://doi.org/10.1088/0957-4484/ 20/23/235502.

[23] S.J. Young, Z.D. Lin, Ethanol gas sensors based on multi-wall carbon nanotubes on oxidized Si substrate, Microsyst. Technol. (2018), https://doi.org/10.1007/s00542-016-3154-2.

[24] C.Y. Zhi, X.D. Bai, E.G. Wang, Enhanced field emission from carbon nanotubes by hydrogen plasma treatment, Appl. Phys. Lett. (2002), https://doi.org/10.1063/1. 1503175.

[25] H. Bubert, S. Haiber, W. Brandl, G. Marginean, M. Heintze, V. Bruser, Characterization of the uppermost layer of plasma-treated carbon nanotubes, Diam. Relat. Mater. (2003), https://doi.org/10.1016/S0925-9635(02)00353-9.

[26] F. Pourfayaz, A.A. Khodadadi, Y. Mortazavi, S.H. Jafari, Plasma functionalization of MWCNTs in he followed by NH3 treatment and its application in PMMA based nanocomposites, Plasma Process. Polym. (2010), https://doi.org/10.1002/ppap. 201000055.

[27] N. Santhosh, G. Filipič, E. Tatarova, O. Baranov, H. Kondo, M. Sekine, M. Hori, K.Ostrikov, U. Cvelbar, Oriented carbon nanostructures by plasma processing: recent advances and future challenges, Micromachines. 9 (2018) 565, https://doi. org/10.3390/mi9110565.

[28] M.L.Y. Sin, G.C.T. Chow, C.K.M. Fung, W.J. Li, P. Leong, K.W. Wong, T. Lee, Ultra-low-power alcohol vapor sensors based on multi-walled carbon nanotube, Proc. 1st IEEE Int. Conf. Nano Micro Eng. Mol. Syst. 1st IEEE-NEMS, 2006, pp. 1198-1202, , https://doi.org/10.1109/NEMS.2006.334679.

[29] L. Valentini, C. Cantalini, I. Armentano, J.M. Kenny, L. Lozzi, S. Santucci, Highly sensitive and selective sensors based on carbon nanotubes thin films for molecular detection, Diam. Relat. Mater. (2004), https://doi.org/10.10167j.diamond.2003. 11.011.

[30] J. Li, Y. Lu, Q. Ye, M. Cinke, J. Han, M. Meyyappan, Carbon nanotube sensors for gas and organic vapor detection, Nano Lett. (2003), https://doi.org/10.1021/ nl034220x.

[31] I.V. Zaporotskova, N.P. Boroznina, Y.N. Parkhomenko, L.V. Kozhitov, Carbon nanotubes: sensor properties. A review, Mod. Electron. Mater. (2016), https://doi. org/10.1016/j.moem.2017.02.002.

[32] P. Slobodian, P. Riha, A. Lengalova, P. Saha, Compressive stress-electrical conductivity characteristics of multiwall carbon nanotube networks, J. Mater. Sci. (2011), https://doi.org/10.1007/s10853-010-5202-0.

[33] N.M. Santhosh, G. Filipič, E. Kovacevic, A. Jagodar, J. Berndt, T. Strunskus, H. Kondo, M. Hori, E. Tatarova, U. Cvelbar, N-graphene nanowalls via plasma nitrogen incorporation and substitution: the experimental evidence, Nano-Micro Lett. 12 (2020) 53, https://doi.org/10.1007/s40820-020-0395-5.

[34] M. Scardamaglia, C. Struzzi, F.J. Aparicio Rebollo, P. De Marco, P.R. Mudimela, J.F. Colomer, M. Amati, L. Gregoratti, L. Petaccia, R. Snyders, C. Bittencourt, Tuning electronic properties of carbon nanotubes by nitrogen grafting: chemistry and chemical stability, Carbon N. Y. (2015), https://doi.org/10.1016/jLcarbon. 2014.11.009.

[35] R.J. Nemanich, S.A. Solin, First- and second-order Raman scattering from finite-size crystals of graphite, Phys. Rev. B (1979), https://doi.org/10.1103/PhysRevB.20. 392.

[36] D. Roy, M. Chhowalla, H. Wang, N. Sano, I. Alexandrou, T.W. Clyne, G.A.J. Amaratunga, Characterisation of carbon nano-onions using Raman spectroscopy, Chem. Phys. Lett. (2003), https://doi.org/10.1016/S0009-2614(03) 00523-2.

[37] M.S. Dresselhaus, G. Dresselhaus, R. Saito, A. Jorio, Raman spectroscopy of carbon nanotubes, Phys. Rep. (2005), https://doi.org/10.1016/j.physrep.2004.10.006.

[38] A.C. Ferrari, D.M. Basko, Raman spectroscopy as a versatile tool for studying the properties of graphene, Nat. Nanotechnol. 8 (2013) 235-246, https://doi.org/10. 1038/nnano.2013.46.

[39] K.M. Daniels, B.K. Daas, N. Srivastava, C. Williams, R.M. Feenstra, T.S. Sudarshan, M.V.S. Chandrashekhar, Evidences of electrochemical graphene functionalization and substrate dependence by Raman and scanning tunneling spectroscopies, in: J, Appl. Phys. (2012), https://doi.org/10.1063Z1.4725489.

[40] F.A. Abuilaiwi, T. Laoui, M. Al-Harthi, M.A. Atieh, Modification and functionalization of multiwalled carbon nanotube (MWCNT) via fischer esterification, Arab. J. Sci. Eng. 35 (2010) 37-48.

[41] S.C. Her, C.Y. Lai, Dynamic behavior of nanocomposites reinforced with multiwalled carbon nanotubes (MWCNTs), Materials (Basel). (2013), https://doi.org/10. 3390/ma6062274.

[42] D.S. Ahmed, A.J. Haider, M.R. Mohammad, Comparesion of functionalization of multi-walled carbon nanotubes treated by oil olive and nitric acid and their characterization, Energy Procedia, 2013, https://doi.org/10.1016/j.egypro.2013.07. 126.